Chapter 3
Electron Kappa Distributions in the Solar Wind: Cause of the Acceleration or Consequence of the Expansion?

Milan Maksimovic, Andrew P. Walsh, Vivienne Pierrard, Štěpán Štverák, and Iannis Zouganelis

Abstract The electron velocity distribution functions in the solar wind, far from the Sun, clearly exhibit a Kappa-like suprathermal tail. Is this characteristic also present in the corona or is it simply the consequence of the solar wind expansion? We elaborate around this question in this short chapter by relying, among others, on the recent electron measurements, as close as 29 solar radii (R_{Sun}) from the Sun, by the Parker Solar Probe.

3.1 Introduction

The power and the beauty of in-situ measurements in space plasmas is that they allow to access directly to the velocity distribution functions (VDFs) of the constituent particles. This privilege is, for example, not reserved for plasma

M. Maksimovic (✉)
LESIA, Observatoire de Paris, Université PSL, CNRS, Sorbonne Université, Unversité de Paris, Meudon, France
e-mail: milan.maksimovic@obspm.fr

A. P. Walsh · I. Zouganelis
ESA, ESAC, Madrid, Spain
e-mail: Andrew.Walsh@esa.int; Yannis.Zouganelis@esa.int

V. Pierrard
Royal Belgian Institute for Space Aeronomy, STCE and Space Physics, Brussels, Belgium

Center for Space Radiations (CSR) and Georges Lemaitre Centre for Earth and Climate Research (TECLIM), Earth and Life Institute (ELI), Université Catholique de Louvain (UCLouvain), Louvain-La-Neuve, Belgium
e-mail: viviane.pierrard@aeronomie.be

Š. Štverák
Czech Academy of Sciences, Astronomical Institute and Institute of Atmospheric Physics, Prague, Czech Republic
e-mail: stepan.stverak@asu.cas.cz

M. Lazar, H. Fichtner (eds.), *Kappa Distributions*, Astrophysics and Space Science Library 464, https://doi.org/10.1007/978-3-030-82623-9_3

measurements in tokamaks. In the latter case, the size of the system is comparable to that of potential measuring instruments. Therefore, complex diagnostic techniques, external to the system, must be used to simply measure the first moments of the distribution functions.

When we thus equip a space probe, exploring the inner heliosphere, with an electrostatic electron analyzer, we realize that the VDF of the latter is unmistakably non-Maxwellian (Vasyliunas 1968; Feldman et al. 1975; Rosenbauer et al. 1977; Pilipp et al. 1987; Maksimovic et al. 1997b). Indeed at Earth orbit, the solar wind electrons are best modeled by a sum of three components: an usually bi-Maxwellian core, a halo population which is a nearly isotropic Kappa distribution (Maksimovic et al. 2005; Štverák et al. 2009; Wilson et al. 2019) and a field-aligned strahl (Rosenbauer et al. 1977) which is also Kappa at large distances from the Sun (Štverák et al. 2009). The Kappa or Lorentzian nature of halo electron velocity distribution functions (eVDFs) is hardly called into question by the observations, as we detail it in the next section. On the other hand, the origin of these Lorentzians, which are observed in the interplanetary medium is not clear. Are such distributions already present in the corona, potentially explaining the heating of the latter (Scudder 1992a,b) and the acceleration of the solar wind (Maksimovic et al. 1997a; Lamy et al. 2003; Zouganelis 2008)? Or is the corona necessarily Maxwellian given the degree of collisionality in the Sun's chromosphere? If this second scenario turns out to be the correct one, then it is necessary to find a physical mechanism which perturbs this thermodynamic equilibrium and creates VDFs which, not only are non-thermal but are in addition extremely close to a Lorentzian for the halo, beyond a certain distance to the Sun.

In this short chapter we discuss the above questions in the context of the latest observations of the solar wind eVDFs, measured as close as 29 R_{Sun} from the Sun by the Parker Solar Probe (PSP) (Fox et al. 2016).

3.2 Typical Examples of Solar Wind Electron Velocity Distribution Functions Observed at 1 au

Figure 3.1 displays a typical eVDF observed in the solar wind, on June 19, 1995, by the WIND-3DP instrument (Lin et al. 1995), located at 1 au. Reaching such a wide energy range, up to 3 keV, and such a large dynamical range for the particle flux, about 10 orders of magnitude, is not common for most of the electron instruments which have flown in the solar wind. For the 3DP instrument, this was only made possible by combining both an electrostatic analyzer for the thermal part of the distributions and solid state detectors for the suprathermal part (Lin et al. 1995). As can be seen in Fig. 3.1 the intercalibration of the two energy ranges is excellent. The blue and black dots represent cuts of the VDF respectively parallel $F_{\parallel}$ and perpendicular $F_{\perp}$ to the local magnetic field. The black full line represents a Maxwellian fit of the thermal part of the VDF, up to 70 eV, for which we exclude

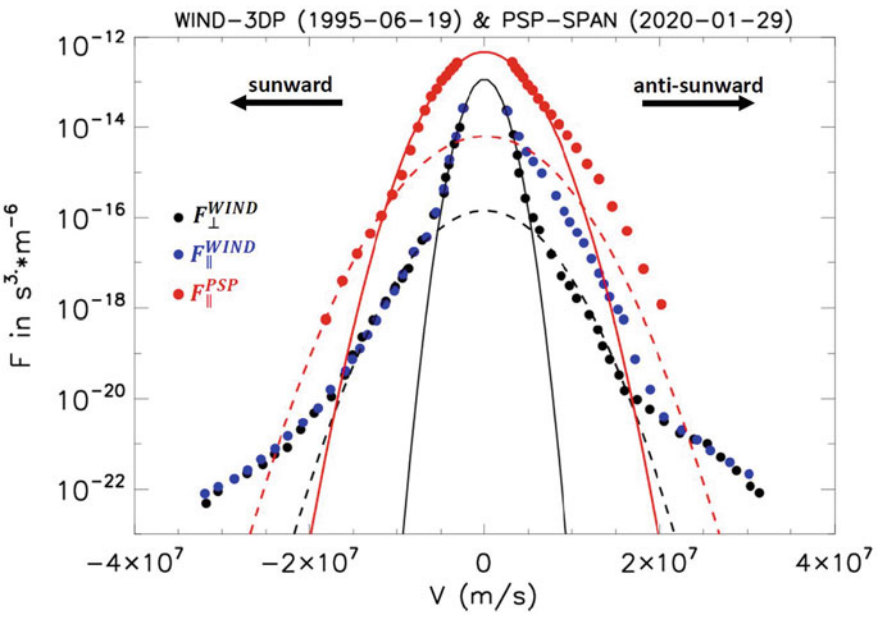

Fig. 3.1 Typical example of an eVDF observed in the solar wind by the WIND-3DP instrument. The blue and black dots represent respectively $F_{\parallel}$ and $F_{\perp}$. The full and dashed black lines represents Maxwellian fits which are discussed in the text. Superimposed with red dots a VDF observed by the SPAN instrument on the PSP located at 29 R_{Sun}. See text for more details

the anti-sunward part of $F_{\parallel}$, in order for the fit to not be influenced by the low energy strahl electrons. The black dashed line represents a Maxwellian fit of the halo part of the VDF, from ∼70 to ∼1400 eV, excluding again the anti-sunward part of $F_{\parallel}$. It is interesting to note, by passing, that we obtain ratios between the densities $N_{halo}/N_{core} \sim 0.03$ and the temperatures $T_{halo}/T_{core} \sim 7.7$ of the halo and core populations which are in the ranges usually observed (Feldman et al. 1975; Phillips et al. 1993; Maksimovic et al. 1995, 1998).

The example in Fig. 3.1 clearly demonstrates that a function consisting of the sum of two Maxwellians does not allow to correctly model the distribution over the whole energy range of its suprathermal part. Beyond ∼1000 eV the observed distribution deviates strongly from the model. As already mentioned, the halo part of the eVDFs is indeed best modelled by a Kappa distribution (Maksimovic et al. 2005; Štverák et al. 2009; Wilson et al. 2019). This can be observed either with the WIND spacecraft, which is equipped with the adequate instrumentation, or with the Ulysses one beyond 1 au (Maksimovic et al. 2005). In this latter case, this property can be observed thanks to the overall decrease of the total electron temperature. This decrease, the instrument energy coverage being constant, allows to have more data points for the halo electrons at high energy with respect to the core thermal energy. This then clearly reveals the Kappa nature of the electron halo.

In Fig. 3.1 we have overplotted a typical eVDF observed with the SWEAP/SPAN electron analyzer (Kasper et al. 2016) on PSP on January 29, 2020, when the probe was at 29 R_{Sun} from the Sun. The red old represent $F_{\parallel}$. The red full and dashed lines represent the Maxwellian fits of respectively the core and the halo populations. As we can see, a model consisting of the sum of two Maxwellian fits nicely the sunward part of the SPAN $F_{\parallel}$, even though the halo population occur to be visible on only a few velocity channels. Contrary to the WIND/3DP case, the SPAN energy range is unfortunately not wide enough to exhibit any departure from the Maxwellian for the halo. We come back to this point in the next sections.

3.2.1 Non Maxwellian Core Electrons

Although the standard model for the solar wind eVDFs is that of a Maxwellian core with Kappa distribution functions for the halo and strahl, recent observations from WIND (Wilson et al. 2019) have revealed that the core is not always Maxwellian. Indeed, observations in the core energy range are sometimes consistent with a Kappa distribution as illustrated in Fig. 3.2. This figure displays a cut of the 3D electron distribution function taken by the PEACE instrument (Johnstone et al.

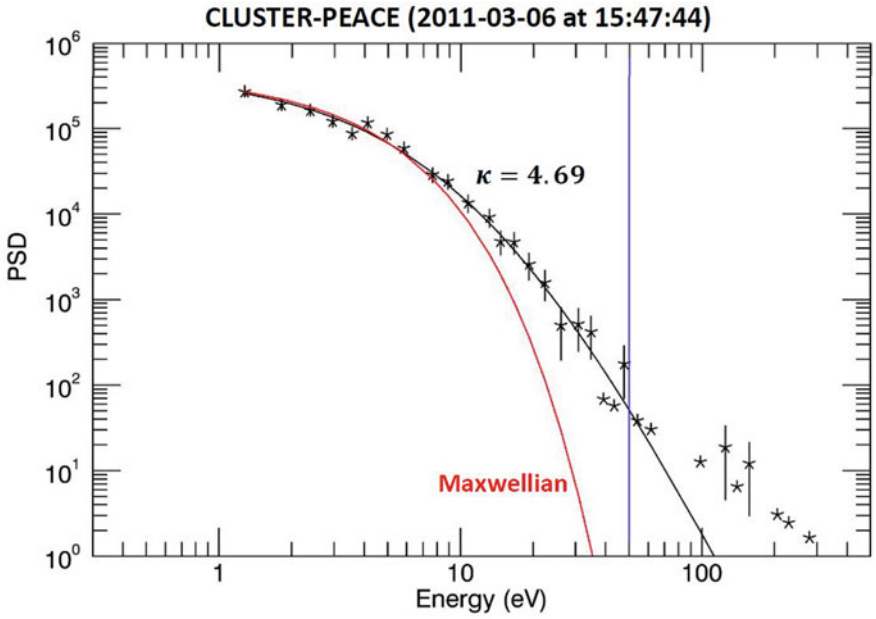

Fig. 3.2 Perpendicular cut of an eVDF taken by the CLUSTER/PEACE instrument in the pristine solar wind. Two fits are included on the plot, a Maxwellian in red and a Kappa in black (see text for more details)

1997; Fazakerley et al. 2010) on one of the CLUSTER spacecraft, while the latter was in the pristine solar wind. The cut is in the perpendicular direction so does not contain any strahl electrons. Data are represented by the asterisks with error bars which are calculated from the counting statistics. Two fits are included on the plot, a Maxwellian in red and a Kappa in black.

Each fit was carried out using a nonlinear least squares algorithm (Markwardt 2009). To do so, as robustly as possible, we express both the data and the model functions in terms of count rate and measured particle energy. This means we can successfully fit in linear, rather than logarithmic, space and also simply use the Poisson error on the count rate to weight the fits. This approach also simplifies the use of the χ^2 statistic to assess the goodness-of-fit. The Kappa and Maxwellian distributions are expressed in terms of count rate as follows

$$R_M(E) = \frac{E_{obs}^2}{G} A e^{-\frac{E_{obs}-E_\phi}{E_0}} \tag{3.1}$$

$$R_\kappa(E) = \frac{E_{obs}^2}{G} A \left(1 + \frac{E_{obs} - E_\phi}{\kappa E_0}\right)^{-\kappa-1} \tag{3.2}$$

Here $R_\kappa(E)$ is the Kappa-distributed count rate and $R_M(E)$ the Maxwell-distributed count rate; E_{obs} is the observed electron energy; G the instrument geometric factor, itself composed of energy-independent and energy-dependent components (see for example Collinson et al. 2012); A is a constant that controls the amplitude of the distribution function and is related to the electron density; E_ϕ is the energy gained by electrons passing through the spacecraft potential; E_0 is the most probable particle energy, i.e. the peak value of the differential particle flux; κ is the kappa index. Of these quantities, R_κ, R_M, E_{obs}, G and E_ϕ are known from the data and instrument characteristics; thus the fitted parameters are A, E_0 and κ.

The details of the fitting procedure are out of the scope of the present chapter and will be presented in a future work. What can be clearly seen, for this particular example in Fig. 3.2, is that at energies lower than the spectral break ($\sim$50 eV) above which the halo can be seen, the measured electrons are better represented by a Kappa distribution than by a Maxwellian. This conclusion is made possible by the property of the PEACE instrument to have a very good energy resolution for the thermal part of the distributions.

At least 10% of the electron distributions observed with the CLUSTER/PEACE instruments in the pristine solar wind have core electrons which are better represented by a Kappa distribution than by a Maxwellian. The reason for this property is unclear and is under investigation.

3.3 Are the Electron Velocity Distributions Functions Maxwellians in the Solar Corona and Become Kappa-Like as the Wind Expands?

There is now a lot of evidences tending to show that the following scenario is the most viable one in order to explain the properties of solar wind eVDFs and their radial evolution in the heliosphere.

1. As the solar wind leaves the corona, the highly collisionless electrons can escape from the ambipolar thermoelectric field (Lemaire and Scherer 1971; Jockers 1970) and create the strahl. In the mean time the thermal electrons, which are both weakly collisional and bounded by the ambipolar potential, create the core (Feldman et al. 1975; Scudder et al. 1979; Scudder and Olbert 1979; Maksimovic et al. 1997a; Scudder 2019; Berčič et al. 2021).
2. At some radial distance from the Sun, which we can hope will be explored by the PSP, the strahl electrons become unstable and trigger waves (Verscharen et al. 2019), such as for instance whistler waves (Vocks et al. 2005; Pierrard et al. 2011; Kajdič et al. 2016; Jagarlamudi et al. 2020; Berčič et al. 2021; Kretzschmar et al. 2021; Vocks 2021), which will have two effects.
3. The first effect will consist in stopping the focusing of the collisionless strahl along the magnetic field lines and, on the contrary, will diffuse it in pitch angles (Hammond et al. 1996; Graham et al. 2017; Berčič et al. 2019).
4. The second effect of the strahl-generated waves will consist in depleting the latter and producing the halo population (Maksimovic et al. 2005; Štverák et al. 2009; Berčič et al. 2019)

Note that in the above scenario the role of the waves in the isotropization of the strahl could also be played by the magnetic turbulence as suggested observationally by Pagel et al. (2007). The most convincing observational evidence that the halo population is generated from the strahl one, probably by some pitch angle scattering mechanism, has been given by Štverák et al. (2009). In Fig. 3.3 we reproduce the Fig. 4 from Štverák et al. (2009), which displays the radial evolution of the relative densities of the eVDF components. The total number of nonthermal electrons remains almost constant along the observed range. The strahl relative density decreases, while the halo one concurrently grows, indicating electrons scattering between these two components.

Furthermore, not only the halo electrons relative density is increasing with distance but its Kappa-like nature is more and more pronounced. This can be seen in Fig. 3.4, which is the reproduction of Fig. 5 from Štverák et al. (2009). In this study the authors have fitted both the halo and the strahl populations with Kappa distribution functions. Figure 3.4 displays the parameter κ of the halo (solid line with diamonds) and strahl (dashed line with circles) components. Both of them are decreasing with radial distance, indicating stronger eVDF tails at larger distances from the Sun.

Finally, a last clue of the radial transformation of the halo into a Kappa distribution is provided by Fig. 3.5. This figure is based on the same representation

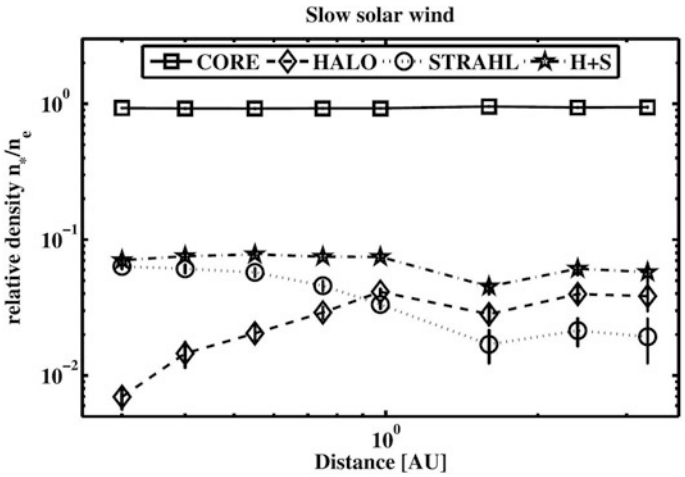

Fig. 3.3 Radial evolution of the relative densities of the eVDF components for the slow solar wind observations. Symbols represent mean values with their error bars. The solid line with squares, dashed line with diamonds, dotted line with circles, and dash-dotted line with stars represent the core, halo, strahl, and sum of strahl and halo, respectively. The total number of nonthermal electrons remains almost constant along the observed range. The strahl relative density decreases, while the halo one concurrently grows, indicating electrons scattering between these two components (see Štverák et al. 2009 for more details). Reproduced with permission from Štverák et al. (2009). © John Wiley and Sons

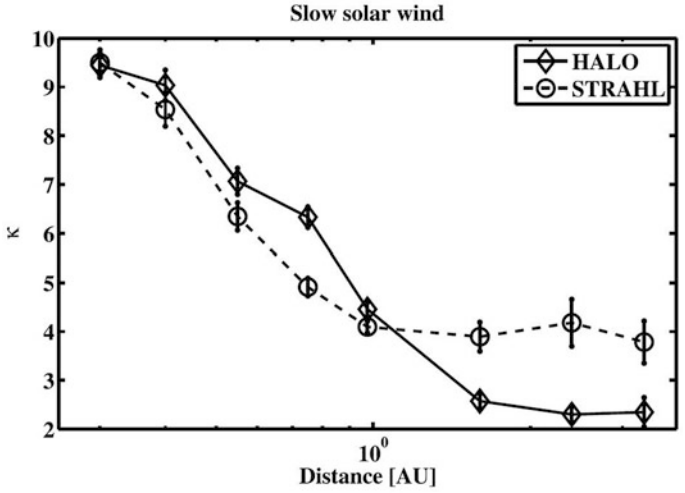

Fig. 3.4 κ parameter of the halo (solid line with diamonds) and strahl (dashed line with circles) components. Both of them are decreasing with radial distance, indicating stronger eVDF tails at larger distances from the Sun (see Štverák et al. 2009 for more details). Reproduced with permission from Štverák et al. (2009). © John Wiley and Sons

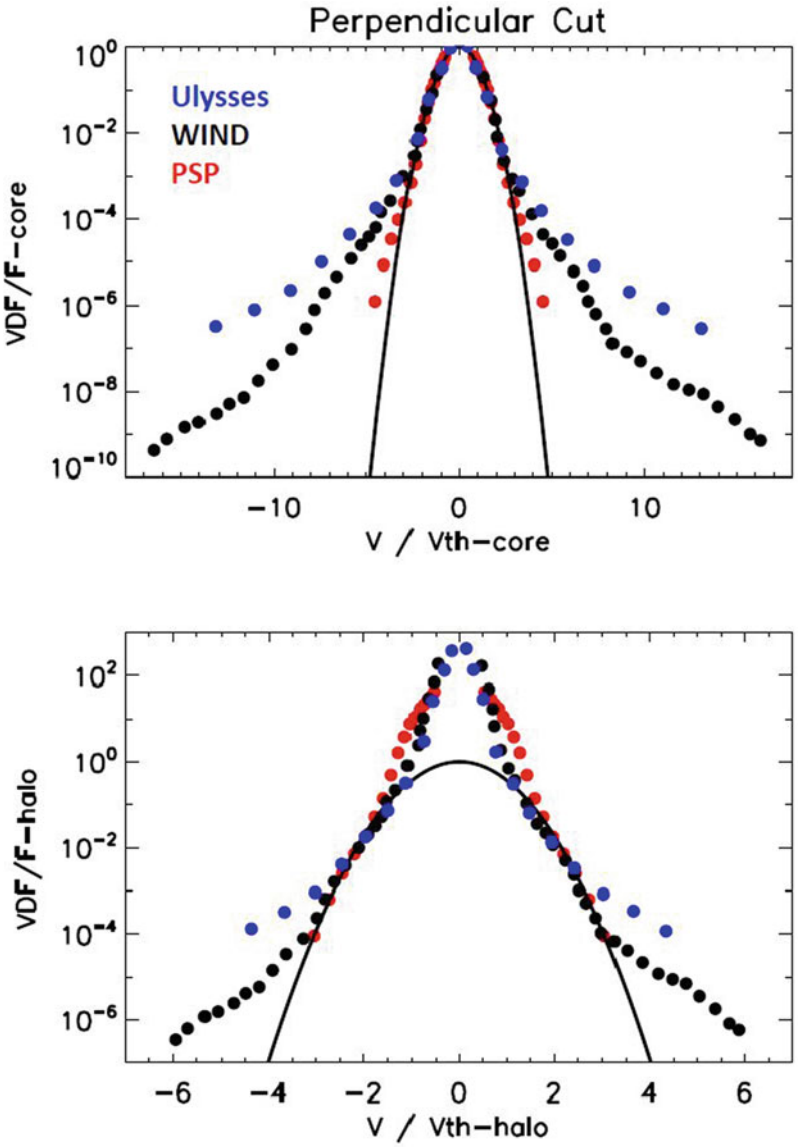

Fig. 3.5 Normalized perpendicular eVDFs cuts for the core (top panel) and the halo (lower panel), in red for the PSP (at 0.13 au), in black for WIND (1 au) and in blue for the Ulysses eVDF, which corresponds to the range 1.35–1.5 au in Fig. 5 from Maksimovic et al. (2005). These normalized $F_{\perp}$ are plotted as function of the velocities normalized by, respectively, the core and the halo Maxwellian thermal speeds

as Fig. 5 in Maksimovic et al. (2005). We display the normalized perpendicular eVDFs cuts for the core (top panel) and the halo (lower panel), in red for the PSP (at 0.13 au), in black for WIND (1 au) and in blue for the Ulysses eVDF, which corresponds to the range 1.35–1.5 au in Fig. 5 from Maksimovic et al. (2005). These normalized $F_{\perp}$ are plotted as function of the velocities normalized by, respectively, the core and the halo Maxwellian thermal speeds. For reference the two solid black lines in the figure are the normalized Maxwellians $\exp(-x^2)$ with $x = v/V_{th-core}$ (top) and $x = v/V_{th-halo}$ (bottom). As one can see on the top panel, the normalized core component remains unchanged at all three radial distances and the relative number of halo electrons, compared to the one of the core, increases with radial distance. Now when the normalization is done with respect to the Maxwellian halo (bottom panel), we can see that the deviation from the Maxwellian at very high speeds is more pronounced on Ulysses than on WIND. It should be noted that, unfortunately, the energy range on PSP does not allow this deviation to be observed at 0.13 au. On PSP the halo component is observed to be Maxwellian (Halekas et al. 2019).

3.4 Are the Electron Velocity Distribution Functions Already Non-Maxwellians in the Solar Corona and Can We Measure This Property in-situ in the Solar Wind?

Indeed there are evidences from the remote-sensing spectroscopic observations of the optically thin parts of the solar atmosphere that the eVDFs are already non-Maxwellians in the solar corona, see Dudík and Dzifčáková (2021) and references therein. If this is the case this would have consequences on the solar wind acceleration. Indeed in solar wind exospheric models (Maksimovic et al. 1997a; Zouganelis 2008; Lamy et al. 2003) nonthermal eVDFs in the corona can accelerate the solar wind by means of the increased ambipolar electric field with respect to the Maxwellian case.

Is there any in-situ observational evidence in the inner heliosphere for the presence of non-Maxwellian eVDFs in the corona? The only one that comes to mind is the strahl parallel temperature and overall shape. Indeed Berčič et al. (2020) have investigated how well the fast and collisionless strahl electrons preserve the information about the coronal electron temperature at their origin. Berčič et al. (2020) have shown that, because of their collisionless nature, the strahl electrons have an equivalent temperature which is independent of radial distance, with values in agreement with coronal temperatures measured using spectroscopic observations (David et al. 1998). Furthermore, Berčič et al. (2020) have confirmed the electron strahl temperature to be anti-correlated with the solar wind velocity, as already reported for the total temperature (Geiss et al. 1995; Gloeckler et al. 2003; Halekas et al. 2019; Maksimovic et al. 2020).

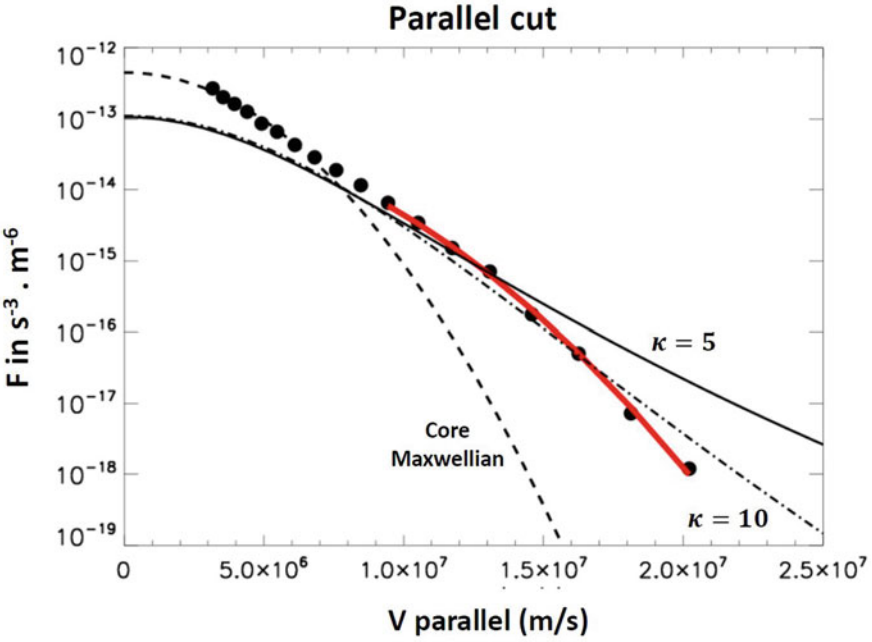

Fig. 3.6 The PSP anti-sunward $F_{\parallel}$, measured at 29 R_{Sun}, is displayed using dots. The dashed line is the Maxwellian fit of the core population. The solid red line is a Maxwellian fit of the strahl yielding a temperature of 1.2 10^6 K. The solid line represents a Kappa distribution with $\kappa = 5$, having the same temperature of 1.2 10^6 K. The dotted-dashed line represents a Kappa with $\kappa = 10$ and a temperature of 10^6 K

An illustration on how the strahl can be used to infer the coronal temperature is shown in Fig. 3.6. In this figure we have displayed, using dots, the PSP anti-sunward $F_{\parallel}$ measured at 29 R_{Sun}. The dashed line is the Maxwellian fit of the core population. The solid red line is the result of a Maxwellian fit of the strahl portion of $F_{\parallel}$ over a velocity range which is indicated by the x-range of the solid lines. As can be seen, the strahl $F_{\parallel}$ is very nicely Maxwellian, as already reported by Berčič et al. (2020). We obtain a temperature of 1.2 10^6 K for this Maxwellian, compatible with typical coronal electron temperature. While the strahl can be used to measure the coronal temperature, it should also provide information on the shape of the coronal eVDFs which, in the absence of collisions, should remain unchanged as the wind expands. This should be all the more true as we approach the Sun, in regions where the strahl has not yet been diffused in pitch angle.

We have checked this latter point by overplotting two Kappa distributions in Fig. 3.6. The solid line represents a Kappa distribution with $\kappa = 5$, having the same temperature as the Maxwellian strahl. The dotted-dashed line represents a Kappa with $\kappa = 10$ and a temperature of 10^6 K. This latter function is quite close to the observed strahl, given the energy range of the PSP SPAN analyzer. Even though a Kappa distribution with $\kappa = 10$ is very close to a Maxwellian, it is different from

this latter. More data, especially in the fast solar wind, are therefore still needed from the PSP in order to conclude on whether or not non-Maxwellian eVDFs can be inferred for the corona, from in-situ measurements in the solar wind.

Acknowledgement M. Maksimovic thanks Laura Berčič for her help with the PSP/SPAN data.

References

L. Berčič, D. Verscharen, C.J. Owen, L. Colomban, M. Kretzschmar, T. Chust, M. Maksimovic, D.O. Kataria, C. Anekallu, E. Behar, M. Berthomier, R. Bruno, V. Fortunato, C.W. Kelly, Y.V. Khotyaintsev, G.R. Lewis, S. Livi, P. Louarn, G. Mele, G. Nicolaou, G. Watson, R.T. Wicks, Astron. Astrophys. (2021)

L. Berčič, Maksimović, M. , S. Landi, L. Matteini, MNRAS **486**(3), 3404 (2019). https://doi.org/10.1093/mnras/stz1007

L. Berčič, D. Larson, P. Whittlesey, M. Maksimović, S.T. Badman, S. Landi, L. Matteini, S.D. Bale, J.W. Bonnell, A.W. Case, T. Dudok de Wit, K. Goetz, P.R. Harvey, J.C. Kasper, K.E. Korreck, R. Livi, R.J. MacDowall, D.M. Malaspina, M. Pulupa, M.L. Stevens, *Astrophys. J.* **892**(2), 88 (2020). https://doi.org/10.3847/1538-4357/ab7b7a

L. Berčič, S. Landi, M. Maksimović, J. Geophys. Res. (Space Physics) **126**(3), e28864 (2021). https://doi.org/10.1029/2020JA028864

G.A. Collinson, J.C. Dorelli, L.A. Avanov, G.R. Lewis, T.E. Moore, C. Pollock, D.O. Kataria, R. Bedington, C.S. Arridge, D.J. Chornay, U. Gliese, A. Mariano, A.C. Barrie, C. Tucker, C.J. Owen, A.P. Walsh, M.D. Shappirio, M.L. Adrian, Rev. Sci. Instrum. **83**(3), 033303 (2012). https://doi.org/10.1063/1.3687021

C. David, A.H. Gabriel, F. Bely-Dubau, A. Fludra, P. Lemaire, K. Wilhelm, Astron. Astrophys. **336**(3), 90 (1998)

J. Dudík, E. Dzifčáková, *Diagnostics of Kappa-Distributions from Optically Thin Solar Spectra, in this book* (2021)

A.N. Fazakerley, A.D. Lahiff, R.J. Wilson, I. Rozum, C. Anekallu, M. West, H. Bacai, *PEACE Data in the Cluster Active Archive* (Springer, Dordrecht, 2010), pp. 129–144. https://doi.org/10.1007/978-90-481-3499-1_8

W.C. Feldman, J.R. Asbridge, S.J. Bame, M.D. Montgomery, S.P. Gary, J. Geophys. Res. **80**(31), 4181 (1975). https://doi.org/10.1029/JA080i031p04181

N.J. Fox, M.C. Velli, S.D. Bale, R. Decker, A. Driesman, R.A. Howard, J.C. Kasper, J. Kinnison, M. Kusterer, D. Lario, M.K. Lockwood, D.J. McComas, N.E. Raouafi, A. Szabo, Space Sci. Rev. **204**, 7 (2016). https://doi.org/10.1007/s11214-015-0211-6

J. Geiss, G. Gloeckler, R. von Steiger, H. Balsiger, L.A. Fisk, A.B. Galvin, F.M. Ipavich, S. Livi, J.F. McKenzie, K.W. Ogilvie, B. Wilken, Science **268**(5213), 1033 (1995). https://doi.org/10.1126/science.7754380

G. Gloeckler, T.H. Zurbuchen, J. Geiss, J. Geophys. Res. (Space Physics) **108**(A4), 1158 (2003). https://doi.org/10.1029/2002JA009286

G.A. Graham, I.J. Rae, C.J. Owen, A.P. Walsh, C.S. Arridge, L. Gilbert, G.R. Lewis, G.H. Jones, C. Forsyth, A.J. Coates, J.H. Waite, J. Geophys. Res. (Space Physics) **122**(4), 3858 (2017). https://doi.org/10.1002/2016JA023656

J.S. Halekas, P. Whittlesey, D.E. Larson, D. Mcginnis, M. Maksimovic, M. Berthomier, J.C. Kasper, A.W. Case, K.E. Korreck, M.L. Stevens, K.G. Klein, S.D. Bale, R.J. Macdowall, M.P. Pulupa, D.M. Malaspina, Astrophys. J. (2019)

C.M. Hammond, W.C. Feldman, D.J. McComas, J.L. Phillips, R.J. Forsyth, A&A **316**, 350 (1996)

V.K. Jagarlamudi, O. Alexandrova, L. Berčič, T.D. de Wit, V. Krasnoselskikh, M. Maksimovic, Š. Štverák, Astrophys. J. **897**(2), 118 (2020). https://doi.org/10.3847/1538-4357/ab94a1

K. Jockers, Astron. Astrophys. **6**, 219 (1970)
A.D. Johnstone, C. Alsop, S. Burge, P.J. Carter, A.J. Coates, A.J. Coker, A.N. Fazakerley, M. Grande, R.A. Gowen, C. Gurgiolo, B.K. Hancock, B. Narheim, A. Preece, P.H. Sheather, J.D. Winningham, R.D. Woodliffe, Space Sci. Rev. **79**, 351 (1997). https://doi.org/10.1023/A:1004938001388
P. Kajdič, O. Alexandrova, M. Maksimovic, C. Lacombe, A.N. Fazakerley, Astrophys. J. **833**(2), 172 (2016). https://doi.org/10.3847/1538-4357/833/2/172
J.C. Kasper, R. Abiad, G. Austin, M. Balat-Pichelin, S.D. Bale, J.W. Belcher, P. Berg, H. Bergner, M. Berthomier, J. Bookbinder, E. Brodu, D. Caldwell, A.W. Case, B.D. Chandran, P. Cheimets, J.W. Cirtain, S.R. Cranmer, D.W. Curtis, P. Daigneau, G. Dalton, B. Dasgupta, D. DeTomaso, M. Diaz-Aguado, B. Djordjevic, B. Donaskowski, M. Effinger, V. Florinski, N. Fox, M. Freeman, D. Gallagher, S.P. Gary, T. Gauron, R. Gates, M. Goldstein, L. Golub, D.A. Gordon, R. Gurnee, G. Guth, J. Halekas, K. Hatch, J. Heerikuisen, G. Ho, Q. Hu, G. Johnson, S.P. Jordan, K.E. Korreck, D. Larson, A.J. Lazarus, G. Li, R. Livi, M. Ludlam, M. Maksimovic, J.P. McFadden, W. Marchant, B.A. Maruca, D.J. McComas, L. Messina, T. Mercer, S. Park, A.M. Peddie, N. Pogorelov, M.J. Reinhart, J.D. Richardson, M. Robinson, I. Rosen, R.M. Skoug, A. Slagle, J.T. Steinberg, M.L. Stevens, A. Szabo, E.R. Taylor, C. Tiu, P. Turin, M. Velli, G. Webb, P. Whittlesey, K. Wright, S.T. Wu, G. Zank, Space Sci. Rev. **204**(1–4), 131 (2016). https://doi.org/10.1007/s11214-015-0206-3
M. Kretzschmar, T. Chust, V. Krasnoselskikh, D. Graham, L.C. et al., Astron. Astrophys. (2021)
H. Lamy, V. Pierrard, M. Maksimovic, J. Lemaire, J. Geophys. Res. **108**, 1047 (2003)
J. Lemaire, M. Scherer, J. Geophys. Res. **76**, 7479 (1971). https://doi.org/10.1029/JA076i031p07479
R.P. Lin, K.A. Anderson, S. Ashford, C. Carlson, D. Curtis, R. Ergun, D. Larson, J. McFadden, M. McCarthy, G.K. Parks, H. Rème, J.M. Bosqued, J. Coutelier, F. Cotin, C. D'Uston, K.P. Wenzel, T.R. Sanderson, J. Henrion, J.C. Ronnet, G. Paschmann, Space Sci. Rev. **71**(1–4), 125 (1995). https://doi.org/10.1007/BF00751328
M. Maksimovic, S. Hoang, N. Meyer-Vernet, M. Moncuquet, J.L. Bougeret, J.L. Phillips, P. Canu, J. Geophys. Res. **100**(A10), 19881 (1995). https://doi.org/10.1029/95JA01550
M. Maksimovic, V. Pierrard, J.F. Lemaire, Astron. Astrophys. **324**, 725 (1997a)
M. Maksimovic, V. Pierrard, P. Riley, Geophys. Res. Lett. **24**(9), 1151 (1997b). https://doi.org/10.1029/97GL00992
M. Maksimovic, J.L. Bougeret, C. Perche, J.T. Steinberg, A.J. Lazarus, A.F. Viñas, R.J. Fitzenreiter, Geophys. Res. Lett. **25**(8), 1265 (1998). https://doi.org/10.1029/98GL00843
M. Maksimovic, I. Zouganelis, J.Y. Chaufray, K. Issautier, E.E. Scime, J.E. Littleton, E. Marsch, D.J. McComas, C. Salem, R.P. Lin, H. Elliott, J. Geophys. Res. **110**(A9), A09104 (2005). https://doi.org/10.1029/2005JA011119
M. Maksimovic, S.D. Bale, L. Berčič, J.W. Bonnell, A.W. Case, T. Dudok de Wit, K. Goetz, J.S. Halekas, P.R. Harvey, K. Issautier, J.C. Kasper, K.E. Korreck, V.K. Jagarlamudi, N. Lahmiti, D.E. Larson, A. Lecacheux, R. Livi, R.J. MacDowall, D.M. Malaspina, M.M. Martinović, N. Meyer-Vernet, M. Moncuquet, M. Pulupa, C. Salem, M.L. Stevens, Š. Štverák, M. Velli, P.L. Whittlesey, Astrophys. J. Suppl. **246**(2), 62 (2020). https://doi.org/10.3847/1538-4365/ab61fc
C.B. Markwardt, in *Astronomical Data Analysis Software and Systems XVIII*. Astronomical Society of the Pacific Conference Series, vol. 411, ed. by D.A. Bohlender, D. Durand, P. Dowler (Astronomical Society of the Pacific, San Francisco, 2009). Astronomical Society of the Pacific Conference Series, vol. 411, p. 251
C. Pagel, S.P. Gary, C.A. de Koning, R.M. Skoug, J.T. Steinberg, J. Geophys. Res. **112**, A04103 (2007). https://doi.org/10.1029/2006JA011967
J.L. Phillips, S.J. Bame, J.T. Gosling, D.J. McComas, B.E. Goldstein, A. Balogh, Adv. Space Res. **13**(6), 47 (1993). https://doi.org/10.1016/0273-1177(93)90389-S
V. Pierrard, M. Lazar, R. Schlickeiser, Solar Phys. **269**(2), 421 (2011). https://doi.org/10.1007/s11207-010-9700-7
W.G. Pilipp, H. Miggenrieder, M.D. Montgomery, K.H. Mühlhäuser, H. Rosenbauer, R. Schwenn, J. Geophys. Res. **92**(A2), 1075 (1987). https://doi.org/10.1029/JA092iA02p01075

H. Rosenbauer, R. Schwenn, E. Marsch, B. Meyer, H. Miggenrieder, M.D. Montgomery, K.H. Muehlhaeuser, W. Pilipp, W. Voges, S.M. Zink, J. Geophys. Z. Geophys. **42**(6), 561 (1977)
J.D. Scudder, Astrophys. J. **398**, 299 (1992a). https://doi.org/10.1086/171858
J.D. Scudder, Astrophys. J. **398**, 319 (1992b)
J.D. Scudder, Astrophys. J. **885**(2), 138 (2019). https://doi.org/10.3847/1538-4357/ab4882
J.D. Scudder, S. Olbert, J. Geophys. Res.**84**(A11), 6603 (1979). https://doi.org/10.1029/JA084iA11p06603
J.D. Scudder, S. Olbert, J. Geophys. Res. **84**(A6), 2755 (1979). https://doi.org/10.1029/JA084iA06p02755
Š. Štverák, M. Maksimovic, P. Trávníček, E. Marsch, A.N. Fazakerley, E.E. Scime, J. Geophys. Res. **114**, A05104 (2009). https://doi.org/10.1029/2008JA013883
Š. Štverák, M. Maksimovic, P.M. Trávníček, E. Marsch, A.N. Fazakerley, E.E. Scime, J. Geophys. Res. (Space Physics) **114**(A5), A05104 (2009). https://doi.org/10.1029/2008JA013883
V.M. Vasyliunas, *Low-Energy Electrons in the Magnetosphere as Observed by OGO-1 and OGO-3*, vol. 10 (1968), p. 622. https://doi.org/10.1007/978-94-010-3467-8_22
D. Verscharen, B.D.G. Chandran, S.Y. Jeong, C.S. Salem, M.P. Pulupa, S.D. Bale, Astrophys. J. **886**(2), 136 (2019). https://doi.org/10.3847/1538-4357/ab4c30
C. Vocks, Kinetic models of wave-electron interaction in the solar corona and wind, in this book (2021)
C. Vocks, C. Salem, R.P. Lin, G. Mann, Astrophys. J. **627**(1), 540 (2005). https://doi.org/10.1086/430119.
I. Wilson, B. Lynn, L.J. Chen, S. Wang, S.J. Schwartz, D.L. Turner, M.L. Stevens, J.C. Kasper, A. Osmane, D. Caprioli, S.D. Bale, M.P. Pulupa, C.S. Salem, K.A. Goodrich, Astrophys. J. Suppl. **243**(1), 8 (2019). https://doi.org/10.3847/1538-4365/ab22bd
I. Zouganelis, J. Geophys. Res. (Space Physics) **113**(A8), A08111 (2008). https://doi.org/10.1029/2007JA012979